Experimental Investigation of FRCM-Concrete Interfacial Debonding

Lesley H. Sneed, Tommaso D'Antino, and Christian Carloni

Synopsis: This paper presents the results of an experimental study conducted to understand the stress-transfer mechanism of fiber reinforced concrete matrix (FRCM) composites externally bonded to a concrete substrate for strengthening applications. The FRCM composite was comprised of a polyparaphenylene benzobisoxazole (PBO) fiber net and polymer-modified cement-based mortar. Direct shear tests were conducted on specimens with composite strips bonded to concrete blocks. Parameters varied were composite bonded length and bonded width. Results were analyzed to understand the effective bonded length, which can be used to establish the load-carrying capacity of the interface to design the strengthening system. The normalized load carrying-capacity was plotted against the width of the composite strip to study the width effect. Finally, strain gage measurements along the bonded length were used to investigate the stress-transfer mechanism.

Keywords: FRCM, Concrete, Inorganic Matrix, Debonding.

ACI member **Lesley H. Sneed** is an Assistant Professor in the Department of Civil, Architectural, and Environmental Engineering at Missouri University of Science and Technology, Rolla, MO, 65409. Dr. Sneed is an associate member of Joint Committee ACI-ASCE 445, Shear and Torsion. Her research interests include design, rehabilitation, and strengthening of reinforced and prestressed concrete structures.

Tommaso D'Antino is a PhD candidate in Civil and Environmental Engineering Sciences, University of Padova, Italy. His research interests include the use of fiber-reinforced composites for strengthening and retrofitting concrete structures.

Christian Carloni is an Associate Professor in the Department of Architecture at the University of Hartford. Dr. Carloni's research interests include fracture mechanics, masonry structures, and composite materials. Dr. Carloni is a member of ACI Committee 446 and an associate member of ACI Committee 440.

INTRODUCTION

Fiber-reinforced composite systems are increasingly used in civil engineering infrastructure applications for strengthening reinforced concrete structural members. A promising new type of composite comprised of fibers and an inorganic cementitious matrix presents several environmental, structural, and sustainability-related advantages over fiber-reinforced polymer (FRP) composites including better compatibility with the concrete substrate, improved freeze-thaw resistance, lesser influence of temperature and humidity on the composite performance, and simpler construction. Studies in the literature on the behavior of externally-bonded fiber reinforced cementitious matrix (FRCM) composites show that while they can be used successfully in strengthening applications[1-13], their performance is different from FRP composites due to differences in debonding failure mechanisms resulting from complex matrix-fiber bonding characteristics. Debonding failures are critical in strengthening applications since they are generally brittle in nature and usually control the overall performance of the system by triggering global member failure. With FRP composites, it is well known that debonding typically occurs within the concrete substrate. However, limited available research on debonding of FRCM composites suggests that debonding occurs within the matrix as a progressive process resulting in large slips at the matrix-fiber interface[1,5,6,14-16], which entails for increased ductility as compared to FRP composites[14]. In general, the matrix serves several critical purposes: it transmits and distributes shear forces between and along the fibers, and it bonds the composite to the concrete substrate, which is necessary for load sharing. A complete understanding of the mechanism of interfacial stress transfer of FRCM composites externally bonded to concrete is critical to design and has not yet been thoroughly examined. This paper presents the results of an experimental study conducted to understand the stress-transfer mechanism of FRCM composites externally bonded to a concrete substrate. The FRCM composite was comprised of polyparaphenylene benzobisoxazole (PBO) fiber net and polymer-modified cement-based mortar. Results from single-lap shear tests with different bonded lengths and bonded widths are presented and discussed.

EXPERIMENTAL PROGRAM

The experimental program included single-lap (direct) shear tests conducted on concrete block (prism) specimens with an externally-bonded FRCM composite strip. The parameters varied were the bonded length and bonded width of the composite strip. The classical push-pull configuration was adopted in which the composite fibers were pulled while the concrete prism was restrained (Figs. 1 and 2). The dimensions of the concrete prisms were 125 mm width x 125 mm depth x 375 mm length (5 in. x 5 in. x 15 in.). The composite material was comprised of a bidirectional PBO fiber net with longitudinal and transverse fiber bundles and cementitious matrix. The nominal width b^* and average thickness t^* of one longitudinal fiber bundle were 5 mm (0.2 in.) and 0.092 mm (0.0036 in.), respectively. Longitudinal fiber bundles are pointed out in Fig. 2. The matrix was applied only in the bonded region to embed the fibers and bond the composite to the concrete substrate. Fibers were bare outside the bonded area. Two aluminum plates were attached to the end of the fiber strip with a thermosetting epoxy to grip the fibers during testing (Fig. 1). A steel frame that was bolted to the testing machine base was used to restrain the concrete prism. A steel plate was inserted between the steel frame and the top of the prism to distribute the pressure provided by the frame restraint to the concrete prism. Dimensions of the frame are shown in Fig. 1. Tests were conducted under displacement control using a close-loop servo-hydraulic universal testing machine with a 556 kN (125 kip) force and +/- 150 mm (6 in.) stroke capacity. During testing the global slip, defined as the relative displacement between points on the composite strip just outside the bonded area and the concrete prism, was increased at a constant rate of 0.00084 mm/s (0.000033 in./s). Global slip was measured using two linear variable displacement transducers (LVDTs) that were attached to the concrete surface near the edge of the bonded region. The LVDTs reacted off of a thin aluminum Ω-shape bent plate that was attached to the PBO transversal fiber bundle surface adjacent to the beginning of the bonded region as shown in Figs. 1 and 2. The average of the two LVDT measurements was used to control the rate.

The concrete prisms were constructed with normal-weight concrete with portland cement (Type 1) without admixtures. The maximum size of the aggregate was 9.5 mm (0.375 in.). Six 100 mm × 200 mm (4 in. x 8 in.) concrete cylinders were cast from the same batch of concrete to determine the concrete compressive strength and splitting tensile strength in accordance with ASTM C39[17] and ASTM C496[18]. Material properties are provided in Table 1.

From the same batch of matrix used to cast the FRCM composite, ten 50 mm × 100 mm (2 in. x 4 in.) cylinders were cast to determine the compressive and tensile strengths of the matrix in accordance with ASTM C39[17] and ASTM C496[18]. Results are provided in Table 1. Uniaxial tension tests were conducted on fiber samples. Samples with one, four, five, and seven longitudinal fiber bundles were tested, with at least three replicate samples. Uniaxial electrical resistance gages were mounted on the central fiber bundle of several specimens to measure the applied load-strain relation. The maximum force divided by the area of longitudinal fibers was similar irrespective of number of bundles. Table 1 reports the ultimate strength, ultimate strain, and elastic modulus taken as the average of the samples tested. Values of ultimate strength, ultimate strain, and elastic modulus of the PBO fiber reported by the manufacturer are 5.8 GPa (840 ksi), 0.025 and 270 GPa (39,000 ksi), respectively[19]. The values obtained from the tension tests were substantially lower than those reported by the manufacturer, although measured values were quite consistent. However, it should be noted that the methodology used by the manufacturer to test the mechanical properties was different from that used in this study[20]. Thirty-three direct shear tests were performed to study the bond characteristics and stress-transfer mechanism of the FRCM composite. The parameters varied were the bonded length and bonded width of the composite. At least three replicates of each combination of parameters were tested. Specimens were named following the notation DS_X_Y_(S)_Z, where X=bonded length (ℓ) in mm, Y=bonded width (b_1) in mm, S indicates that strain gages were mounted on the specimen, and Z=specimen number (Table 2). The number of longitudinal bundles n is indicated in Table 2.

The surface of the concrete prisms was sandblasted before applying the composite. A layer of cementitious matrix was then applied using molds to control the composite width and thickness. A single layer of PBO fiber net was then applied onto the matrix layer pushing the fibers delicately to assure proper impregnation. The fiber net strip was positioned such that it extended slightly beyond the end of the matrix at the unloaded end as shown in Fig. 2. A second layer of matrix was then applied over the PBO fibers. Each specimen was allowed to cure for at least one week before testing. The thickness of each of the two layers of matrix was 4 mm (0.15 in.) as recommended by the manufacturer[19]. The total thickness of composite t was 8 mm (0.3 in.) as indicated in Table 2.

Five specimens were instrumented with uniaxial electrical resistance strain gages (gage length = 1 mm [0.04 in.]) to study the axial strain distribution along the bonded length of composite. The positions of the strain gages are shown in Fig. 3a. Gages 4-7 were mounted to the fibers along the bonded length of the composite, and Gages 1-3 were mounted to the fibers outside the bonded length. For specimens DS_330_43_S_3, DS_330_43_S_4, and DS_330_43_S_5, Gages 1 and 3 were omitted. All gages were mounted to longitudinal fibers. Two different techniques were used to apply the strain gages to the fibers along the bonded length. For specimens DS_330_43_S_1 and DS_330_43_S_2, slots were created during the application of the top layer of matrix in the locations of the strain gages. Strain gages were then applied to the fibers after the composite set (Fig. 3b). For specimens DS_330_43_S_3, DS_330_43_S_4, and DS_330_43_S_5, strain gages were mounted to the fiber bundles and then embedded in the top layer of matrix (Fig. 3c).

DISCUSSION OF RESULTS

General behavior

Specimens were tested until one of the following conditions occurred: a sudden and drastic reduction in applied load, or considerable slippage between fibers and matrix. In general no damage was observed at the matrix-concrete interface except for specimens DS_100_34_1 and DS_100_34_2. The authors postulate that a Mode-I condition prevailed in these two tests due to the short bonded length adopted[21]. With the exception of specimens DS_100_34_1 and DS_100_34_2, debonding occurred at the matrix-fiber interface. As global slip increased, longitudinal fiber bundles were observed to gradually pull out of the composite at the loaded end of the bonded surface, and longitudinal fibers beyond the end of the bonded length advanced slowly into the matrix (position y=0 in Figure 3a). In many tests, the bare fiber net at the loaded end of the specimen exhibited nonuniform load-sharing among the longitudinal bundles with increasing slip. This was evidenced by global rotation of the Ω-shape bent plate, as well as by deformation observed in the transversal fiber bundles, which were orthogonal to the longitudinal fibers at the start of the test. This observation suggests that redistribution of stress was occurring between longitudinal fiber bundles throughout the test. Some specimens had preexisting shrinkage cracks on the composite surface, especially specimens with strain gages (see Fig. 3b); these cracks opened with increasing slip. The cracks eventually penetrated the thickness of the composite, as could be seen from the side of the specimens. The presence of through-thickness cracks resulted in a discontinuity in the stress transfer between fibers and matrix with consequent localized deformation at the crack locations along the composite bonded length. Cracks were not observed in specimens that did not have prexisiting shrinkage cracks, which suggests a more uniform stress distribution along the composite bonded length, and that failure is controlled by slippage of fibers.

Maximum load and load-global slip response

The maximum load P^* is reported for each test specimen in Table 2. Scatter in the values of P^* can be explained in part by the non-uniform load-sharing among fiber bundles as discussed previously in the description of general behavior. Typical load P-global slip responses for different bonded lengths and widths are shown in Fig. 4. In general, a linear response is followed by a non-linear response up to the peak load. The descending post-peak response is characterized by slippage of the fibers with respect to the matrix. As mentioned previously, tests were terminated when considerable slippage between fibers and matrix was recorded.The stress-transfer mechanism for FRCM composites, including the role of the matrix on each side of the fiber net, is not yet understood. Because the application of strain gages introduced interruptions in the matrix top layer, two different applications were attempted, and the load response relations were compared. Load responses of the specimens with strain gages are reported in Fig. 5. The responses of specimens without strain gages, DS_330_43_1 and DS_330_43_5, are also plotted in Fig. 5 for comparison. The maximum applied load for specimens DS_330_43_S_1, DS_330_43_S_2, and DS_330_43_S_5 is consistent with the results previously discussed. However, in specimens DS_330_43_S_1 and DS_330_43_S_2, the non-linear pre-peak response appears to be more emphasized. It is possible that the slots used to mount the strain gages on specimens DS_330_43_S_1 and DS_330_43_S_2 induced a stress concentration at the gage locations or modified the restraining action of the matrix, which highlights the need to investigate the role of the top layer of matrix. The load response of specimen DS_330_43_S_4 exhibited a sharp decrease in applied load due to localized stretching of the fibers outside the bonded region. In this case the non-uniform distribution of load in the longitudinal bundles caused a localized stress peak leading to the failure of one or more bundles.

Influence of bonded length

Figure 6 shows the relation between maximum load P^* and bonded length ℓ of the composite for the series of test specimens with composite width b_1 of 34 mm (1.3 in.) (corresponding to n=4 bundles). An increasing trend can be seen between maximum load and bonded length, and similar to FRP-concrete joints, increasing bonded lengths result in a less than proportional increase in maximum load. For FRP-concrete joints, an effective bond length l_{eff}, defined as the minimum length of the bonded area in the direction of the fibers to fully establish the load-carrying capacity of the interface, can be determined from this type of relation as the length beyond which the maximum load remains constant. The maximum load associated with l_{eff} is the debonding force. If these same definitions and relations hold for FRCM-composite joints, results from Figure 6 suggest that the effective bond length l_{eff} is in the range of 250 to 350 mm (10 to 13 in.), if in fact it exists for this composite. Experimental results reported by D'Ambrisi et al.[16] using the same composite tested with double-lap shear tests suggested that the effective bond length is approximately 250 to 300 mm (10 to 12 in.), although it should be noted that the longest bonded length tested in that study was 250 mm (10 in.). Further investigation of the effective bond length will be conducted by the authors in the near future including investigation of longer composite bonded lengths and the influence of other stress-transfer mechanisms such as friction. For comparison, the effective bond length l_{eff} was computed using the formulation provided in ACI 440.2R-08[22] for the FRP-concrete interface. Using this approach, however, the computed effective bond length of the FRCM-concrete interface was found to be significantly underestimated. A possible reason is the different debonding mechanism between the FRP-concrete and FRCM-concrete interfaces.

Figure 7 depicts the maximum load P^* normalized with respect of the total width of the longitudinal fiber bundles nb^* versus bonded length ℓ of composite for all specimens with the exception of those with strain gages. Specimens with n=4, 5, and 7 bundles are plotted in the graph. Similar to Fig. 6, the normalized maximum load increases for the entire range of bonded lengths tested, and increasing bonded lengths result in a less than proportional increase in normalized maximum load.

Influence of bonded width

Figure 8 shows the relation between maximum load P^* normalized with respect of the total width of the longitudinal fiber bundles nb^* versus composite bonded width b_1 for test specimens with the same bonded length (ℓ=330 mm [13 in.]). Specimens with strain gages were omitted from the graph. Three different bonded widths are shown, namely 34 mm (1.3 in.), 43 mm (1.7 in.), and 60 mm (2.4 in.). Results show that specimens with different bonded widths have a similar normalized maximum load. This observation is confirmed by results reported by D'Ambrisi et al.[16] of test specimens with the same composite and with a bonded width of 100 mm tested with double-lap shear tests. These results suggest that a width effect does not exist for this type of composite. FRP composite, on the other hand, has been shown to exhibit a width effect[23,24]. FRP and FRCM have several mechanical differences that might explain this difference in phenomenon, such as fiber layouts (sheets with continuous fibers across the width, versus net with discrete fiber bundles across the width) and bonding characteristics of the matrix. The limited data in Fig. 8 also exhibit greater scatter with smaller bonded width. This may be due to limited force redistribution capability in fiber nets with fewer than a certain critical number of bundles. As discussed previously, redistribution of forces was observed in the fiber bundles throughout the test. More data are needed to further investigate this phenomenon.

Measured strain

Axial strains along the direction of the longitudinal fibers ε_{yy} in the central and edge bundles of specimen DS_330_43_S_1 recorded by gages 1, 2, and 3, outside the bonded region, are reported in Fig. 9. Filled markers indicating the average values are shown in the figure, and coefficient of variation values are given in parentheses. Considering the average values of strain, Figure 9 shows that the applied load and the strain in the longitudinal bundles outside the bonded region is approximately linear. If the average stress of the bundles is computed, the results can be used to calculate the elastic modulus of the fibers. Values computed confirm the value determined from the tension tests discussed previously. Figure 9 also shows that a non-uniform strain distribution is observed among the three bundles that were instrumented with strain gages. A similar phenomenon is observed in FRP strips attached to concrete, and it is partially due to the local variation of the interfacial properties. In the case of discrete fiber bundles this phenomenon appears to be more pronounced. The non-uniform strain distribution may also be partially due to a slight eccentricity of the applied load. For load levels less than 50%P^*, it can be seen that the rate of change in strain with increasing applied load is approximately the same for the three bundles instrumented. For load levels higher than 50%P^*, the rate of change in strain is different. This behavior supports the visual observations of non-uniform load sharing of bundles discussed previously and suggests that load redistribution occurs among fiber bundles with increasing slip, even at load levels less than the peak load. The variation of the strain in specimen DS_330_43_S_1 at different locations along the bonded length for different values of the load is depicted in Fig. 10a. Location along bonded length y is defined in Fig. 3a. Note that strain gage 9 was damaged prior to testing, so it is not shown in the figure. Five values of the load, corresponding to five points (A1, B1, C1, D1, and E1) of the load response in Fig. 10b, were considered. The strain profiles of Fig. 10a resemble the profiles obtained from similar tests for FRP-concrete joints[23,24]. This observation suggests that for FRCM-concrete interfaces a cohesive material interfacial law can be obtained. It should be noted that the limited points along the bonded length where strains were measured might lead to an erroneous interpretation of the readings. Additional measurements are planned for future tests to verify the strain profiles and determine if a cohesive material law similar to that used for the FRP-concrete interface can be adapted to the description of the matrix-fiber interface in FRCM composites.

CONCLUSIONS

This paper describes the results of experimental research conducted to study the stress-transfer mechanism of fiber reinforced concrete matrix (FRCM) composites externally bonded to a concrete substrate. The FRCM composite was comprised of a polyparaphenylene benzobisoxazole (PBO) fiber net and polymer-modified cement-based mortar. Direct shear tests were conducted on specimens with composite strips bonded to concrete blocks. Parameters varied were composite bonded length and bonded width. Based on the results of this study, the following conclusions can be made:

1. Debonding of the FRCM composite occurred at the matrix-fiber interface rather than the matrix-concrete interface.
2. For the range of composite bonded lengths tested (100 to 330 mm), an increasing trend was observed between maximum load and bonded length. Similar to FRP-concrete joints, increasing bonded lengths resulted in a less than proportional increase in maximum load. Results obtained thus far suggest that the effective bond length is in the range of 250 to 350 mm (10 to 13 in.), if in fact it exists for this composite.

3. Although a width effect was not observed, specimens with smaller bonded widths exhibited greater scatter with respect to maximum load. This may be due to limited force redistribution capability in fiber sheets with fewer than a certain critical number of bundles.
4. The strain distribution along the bonded length resembles the strain distribution typical of FRP strips bonded to a concrete substrate. Further investigation is needed to determine the existence or value of an effective bond length for this composite based on the strain profiles.

ACKNOWLEDGEMENTS

The experimental work discussed in this paper was conducted at Missouri University of Science and Technology (Missouri S&T). The authors would like to express their appreciation to the National University Transportation Center (NUTC) at Missouri S&T for providing financial support for this project. Ruredil S.p.A. of San Donato Milanese, Italy, is gratefully acknowledged for providing the composite materials.

REFERENCES

1. Pareek, S., Suzuki, Y., and Kobayashi, A., 2007, "Flexural and Shear Strengthening of RC Beams Using Newly Developed CFRP and Polymer-Cement Pastes as Bonding Agents." *8th International Symposium on Fiber Reinforced Polymer Reinforcement for Concrete Structures*, FRPRCS-8, 16-18 July 2007, Patras, Greece.

2. Blanksvärd, T., Täljsten, B., and Carolin, A., 2009, "Shear Strengthening of Concrete Structures with the Use of Mineral-Based Composites." *J. Compos. Constr.*, ASCE, 13(1), 25-34.

3. Johansson, T. and Täljsten, B., 2005, "End Peeling of Mineral Based CFRP Strengthened Concrete Structures – A Parametric Study." *Proc. International Symposium on Bond Behaviour of FRP in Structures (BBFS 2005)*, Chen and Teng (eds), 197-204.

4. Orosz, K., Täljsten, B., and Fischer, G., 2007, "CFRP Strengthening With Mineral Based Composites Loaded In Shear." *8th International Symposium on Fiber Reinforced Polymer Reinforcement for Concrete Structures*, FRPRCS-8, 16-18 July 2007, Patras, Greece.

5. Blanksvärd, T., 2007, "Strengthening of Concrete Structures by the Use of Mineral Based Composites." Licentiate thesis, Luleå Univ. of Technology, Luleå, Sweden.

6. Täljsten, B., and Blanksvärd, T., 2007, "Mineral Based Bonding Of Carbon FRP To Strengthen Concrete Structures." *J. Compos. Constr.*, ASCE, 11(2), 120–128.

7. Toutanji, H., and Deng, Y., 2007, "Comparison between Organic and Inorganic Matrices for RC Beams Strengthened with Carbon Fiber Sheets." *J. Compos. Constr.*, ASCE, 11(5), 507-513.

8. Ombres, L., 2012, "Debonding Analysis of Reinforced Concrete Beams Strengthened with Fibre Reinforced Cementitious Mortar." *Eng. Frac. Mech*. 81, 4-109.

9. D'Ambrisi, A., Focacci F., 2011, "Flexural Strengthening of RC beams with Cement Based Composites." *J. Compos. Constr.,* ASCE, 15(2), 707–20.

10. Ombres, L., 2007, "Confinement Effectiveness in Concrete Strengthened with Fiber Reinforced Cement Based Composite Jackets," *8th International Symposium on Fiber Reinforced Polymer Reinforcement for Concrete Structures*, FRPRCS-8, 16-18 July 2007, Patras, Greece.

11. Peled, A., 2007, "Confinement of Damaged and Nondamaged Structural Concrete with FRP and TRC Sleeves." *J. Compos. Constr.*, ASCE, 11(5), 514-522.

12. Triantafillou TC, Papanicolaou CG, Zissinopoulos P, Laourdekis T., 2006, Concrete confinement with textile-reinforced mortar jackets. *ACI Struct J.,* 103(1), 28–37.

13. Bournas D.A., Triantafillou T.C., Zygouris K., Stavropoulos F., 2009, “Textile-reinforced Mortar Versus FRP Jacketing in Seismic Retrofitting of RC Columns with Continuous or Lap-spliced Deformed Bars.” *J. Compos. Constr.,* ASCE, 13(5), 360–371.

14. Wiberg, A., 2003, “Strengthening of Concrete Beams Using Cementitious Carbon Fibre Composites.” Doctoral thesis, Royal Institute of Technology, Stockholm, Sweden.

15. D’Ambrisi, A., Feo, L., and Focacci, F., 2012, “Bond-slip Relations for PBO-FRCM Materials Externally Bonded to Concrete.” *Compos.: Part B*, 43(8), 2938-2949.

16. D’Ambrisi, A., Feo, L., and Focacci, F, 2012, “Experimental Analysis on Bond Between PBO-FRCM Strengthening Materials and Concrete.” *Compos.: Part B*, 44(1), 524-532.

17. ASTM, 2011, “Standard Test Method for Compressive Strength for Cylindrical Concrete Specimens,” *C39/C39M-12*, ASTM International, 7 pages.

18. ASTM, 2011, Standard Test Method for Splitting Tensile Strength of Cylindrical Concrete Specimens,” *C496/C496M* ASTM International, 5 pages.

19. Ruredil, 2009, *X Mesh Gold Data Sheet*. Ruredil S.p.A, Milan, Italy. http://english.ruredil.it/SchedeProdottoENG/RuredilXMeshGOLD_ing_1.pdf

20. Toyobo, 2005, *Zylon© (PBO Fiber) Technical Information*. Toyobo Co., Ltd., Osaka, Japan. http://www.toyobo-global.com/seihin/kc/pbo/Technical_Information_2005.pdf

21. Yao, J., Teng, J.G., and Chen, J.F., 2005, “Experimental Study on FRP-to-Concrete Bonded Joints,” *Composites: Part B*, V. 36, 99-113.

22. ACI Committee 440, 2008, “Guide for the Design and Construction of Externally Bonded FRP Systems for Strengthening Concrete Structures (*ACI 440.2R-08)*,” American Concrete Institute, Farmington Hills, MI.

23. Subramaniam, K. V., Carloni, C. and Nobile, L., 2007, “Width Effect in the Interface Fracture During Debonding of FRP from Concrete.” *Eng. Frac. Mech.,* 74, 578–594.

24. Subramaniam, K. V., Carloni, C. and Nobile, L., 2011, “An Understanding of the Width Effect in FRP-Concrete Debonding.” *Strain*, 47(2), 127-137.

Table 1—Material Properties

Concrete Prism	
Compressive strength MPa (psi); *COV*	42.5 (6160) *0.013*
Splitting tensile strength MPa (psi); *COV*	3.4 (490) *0.113*
FRCM Composite	
Mortar	
Compressive strength MPa (psi); *COV*	27.9 (4050) *0.009*
Splitting tensile strength MPa (psi); *COV*	3.6 (520) *0.072*
PBO Fibers	
Ultimate strength GPa (ksi); *COV*	3.0 (430) *0.068*
Ultimate strain *COV*	0.0145 *0.104*
Elastic modulus GPa (ksi); *COV*	206 (29,900) *0.065*

Table 2—Test Specimens

Name	Composite Width b_1 mm (in.)	Number of Bundles n	Composite Length ℓ mm (in.)	Composite Thickness t mm (in.)	Maximum Load P^* kN (k)
DS_100_34_1	34 (1.3)	4	100 (4)	8 (0.3)	1.92 (0.43)
DS_100_34_2	34 (1.3)	4	100 (4)	8 (0.3)	0.97 (0.22)
DS_100_34_3	34 (1.3)	4	100 (4)	8 (0.3)	1.62 (0.36)
DS_150_34_1	34 (1.3)	4	150 (6)	8 (0.3)	2.22 (0.50)
DS_150_34_2	34 (1.3)	4	150 (6)	8 (0.3)	1.55 (0.35)
DS_150_34_3	34 (1.3)	4	150 (6)	8 (0.3)	2.87 (0.65)
DS_150_34_4	34 (1.3)	4	150 (6)	8 (0.3)	2.34 (0.53)
DS_200_34_1	34 (1.3)	4	200 (8)	8 (0.3)	3.05 (0.69)
DS_200_34_2	34 (1.3)	4	200 (8)	8 (0.3)	2.52 (0.57)
DS_200_34_3	34 (1.3)	4	200 (8)	8 (0.3)	3.44 (0.77)
DS_250_34_1	34 (1.3)	4	250 (10)	8 (0.3)	2.61 (0.59)
DS_250_34_2	34 (1.3)	4	250 (10)	8 (0.3)	2.11 (0.47)
DS_250_34_3	34 (1.3)	4	250 (10)	8 (0.3)	2.82 (0.63)
DS_330_34_1	34 (1.3)	4	330 (13)	8 (0.3)	3.00 (0.67)
DS_330_34_2	34 (1.3)	4	330 (13)	8 (0.3)	3.51 (0.79)
DS_330_34_7	34 (1.3)	4	330 (13)	8 (0.3)	4.07 (0.91)
DS_330_34_8	34 (1.3)	4	330 (13)	8 (0.3)	4.02 (0.90)
DS_330_34_9	34 (1.3)	4	330 (13)	8 (0.3)	3.44 (0.77)
DS_330_43_1	43 (1.7)	5	330 (13)	8 (0.3)	4.43 (1.00)
DS_330_43_2	43 (1.7)	5	330 (13)	8 (0.3)	5.25 (1.18)
DS_330_43_3	43 (1.7)	5	330 (13)	8 (0.3)	5.27 (1.18)
DS_330_43_5	43 (1.7)	5	330 (13)	8 (0.3)	4.79 (1.08)
DS_330_43_6	43 (1.7)	5	330 (13)	8 (0.3)	5.09 (1.14)
DS_330_43_S_1	43 (1.7)	5	330 (13)	8 (0.3)	4.48 (1.01)
DS_330_43_S_2	43 (1.7)	5	330 (13)	8 (0.3)	5.12 (1.15)
DS_330_43_S_3	43 (1.7)	5	330 (13)	8 (0.3)	3.03 (0.68)
DS_330_43_S_4	43 (1.7)	5	330 (13)	8 (0.3)	4.60 (1.03)
DS_330_43_S_5	43 (1.7)	5	330 (13)	8 (0.3)	4.03 (0.91)
DS_330_60_1	60 (2.4)	7	330 (13)	8 (0.3)	7.05 (1.59)
DS_330_60_2	60 (2.4)	7	330 (13)	8 (0.3)	6.56 (1.47)
DS_330_60_3	60 (2.4)	7	330 (13)	8 (0.3)	6.06 (1.36)
DS_330_60_4	60 (2.4)	7	330 (13)	8 (0.3)	6.50 (1.46)
DS_330_60_5	60 (2.4)	7	330 (13)	8 (0.3)	6.28 (1.41)

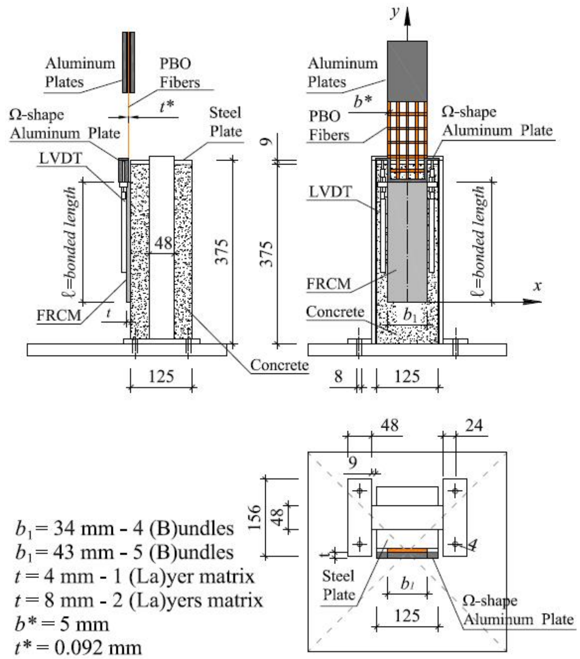

Figure 1 — Test setup (dimensions in mm; 1 mm = 0.0394 in.)

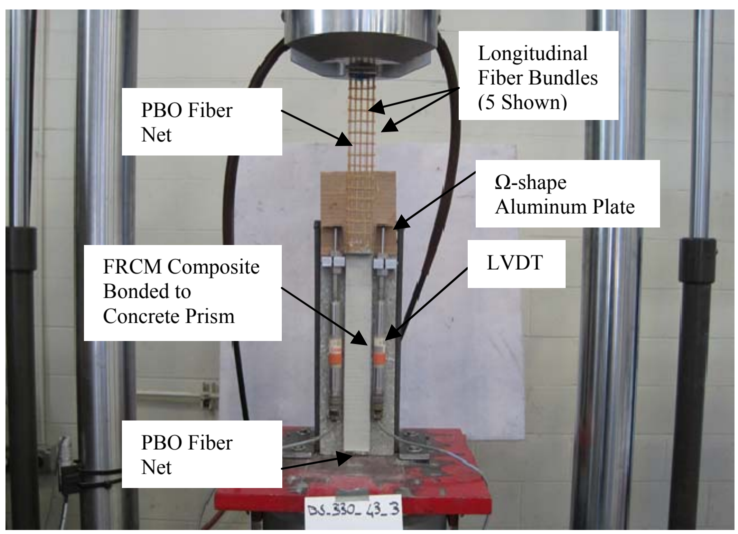

Figure 2 — Photo of specimen DS_330_43_3